Biopolymers

WILEY

Biopolymers

ARTICLE

Nicotinic Acid–Modified Chitosan Nanoparticles for Enhanced Resveratrol Delivery and Anticancer Activity

Sema Şentürk[1,2] | Özlem Kaplan[3] | Kevser Bal[2] | Sibel Küçükertuğrul Çelik[2] | Nazan Gökşen Tosun[4] | Mehmet Koray Gök[2]

[1]Department of Chemical Engineering, Istanbul Health and Technology University, Faculty of Engineering and Natural Sciences, Istanbul, Türkiye | [2]Department of Chemical Engineering, Istanbul University-Cerrahpaşa, Faculty of Engineering, Istanbul, Türkiye | [3]Department of Genetics and Bioengineering, Alanya Alaaddin Keykubat University, Rafet Kayış Faculty of Engineering, Antalya, Türkiye | [4]Department of Medical Services and Techniques, Tokat Gaziosmanpaşa University, Tokat Vocational School of Health Services, Tokat, Türkiye

Correspondence: Mehmet Koray Gök (mkgok@iuc.edu.tr)

Received: 12 December 2025 | **Revised:** 28 January 2026 | **Accepted:** 4 February 2026

Keywords: cancer therapy | chitosan | drug delivery | nicotinic acid | resveratrol

ABSTRACT

This study focused on functionalizing chitosan with nicotinic acid, the active form of vitamin B3, to obtain a new derivative (Chi_{Nico}) with enhanced solubility at physiological pH, improved proton buffering capacity, and in vitro anticancer activity, and to develop resveratrol-loaded nanoparticles ($nChi_{Nico\text{-}RES}$) for enhanced anticancer performance. Chitosan was modified through EDC-mediated amidation, and successful conjugation was confirmed by FTIR, ^{1}H NMR, and GPC/SEC analyses. Nicotinic acid grafting increased molecular weight, introduced characteristic amide signals, improved solubility at physiological pH, and enhanced proton buffering capacity. Nanoparticles were prepared by ionotropic gelation and showed sizes of 100–140 nm, PDI values below 0.4, and a positive surface charge of +18 to +20 mV. Blank nanoparticles exhibited minimal cytotoxicity, while resveratrol-loaded formulations demonstrated significant anticancer activity in HeLa cervical cancer cells and HT-29 human colon adenocarcinoma cell line. Notably, $nChi_{Nico\text{-}RES}$ reduced HeLa and HT-29 cell viability more effectively than free resveratrol and nanoparticles based on unmodified chitosan, indicating an additive contribution from nicotinic acid. In contrast, the cytotoxic effect on healthy BJ fibroblasts remained considerably lower, supporting the biocompatibility and selective potential of the system. Overall, nicotinic acid modification improves chitosan's carrier performance and offers a novel strategy by combining two natural bioactive molecules within a single nanoparticle platform.

1 | Introduction

Cancer remains one of the leading causes of death worldwide, making the development of innovative strategies that can overcome the limitations of current therapies an urgent necessity [1]. The use of conventional chemotherapeutic agents is frequently restricted by issues such as drug resistance and severe side effects on healthy tissues. In this context, nanoparticle-based systems can enhance the therapeutic efficacy of anticancer agents by concentrating them directly at the tumor site, while minimizing adverse effects on healthy tissues [2, 3]. In this field, chitosan, a natural polysaccharide, has been extensively investigated as a drug delivery material owing to its superior properties, including biocompatibility, biodegradability, and its abundance from renewable sources [4]. The use of natural products in cancer therapy has become an attractive research area due to the rising problems of resistance and the side effects of chemotherapeutic drugs. Among these, resveratrol, a natural polyphenol found in foods such as grapes, blueberries, and peanuts, has been intensively studied for its antioxidant, anti-inflammatory, and anticancer properties [5]. Resveratrol can interfere with multiple stages of cancer development, including initiation, progression, and metastasis; it suppresses cell proliferation, induces apoptosis through ROS-mediated mitochondrial pathways, and

inhibits angiogenesis and metastasis. Furthermore, when combined with conventional chemotherapeutic agents, resveratrol has been reported to sensitize tumor cells to these agents and to exert synergistic effects [6, 7]. However, its poor solubility, sensitivity to light, and low bioavailability pose significant challenges for clinical applications [8, 9]. Indeed, resveratrol is not currently approved as a clinical anticancer drug, primarily due to its unfavorable pharmacokinetic properties. Although it exhibits a relatively high oral absorption rate of approximately 75%, rapid first-pass metabolism in the intestine and liver, mainly through glucuronidation and sulfation, results in systemic levels of free resveratrol remaining below 1%. Metabolites generated through these rapid metabolic processes, such as *trans*-resveratrol-3-*O*-glucuronide and *trans*-resveratrol-3-sulfate, further hinder the maintenance of therapeutically relevant concentrations of free resveratrol in the systemic circulation [8, 10, 11]. This limitation makes it difficult to sustainably maintain therapeutically effective plasma concentrations. Clinical studies have reported that, particularly in systemic cancer types, the high doses required to achieve therapeutic levels (e.g., 2.5–5 g per day) are associated with gastrointestinal adverse effects and may pose a risk of serious toxicity in certain patient populations [11]. In addition, the poor aqueous solubility and limited photostability of resveratrol complicate the development of effective pharmaceutical formulations. The most biologically active isomer, *trans*-resveratrol, can undergo photoisomerization upon light exposure, converting into the biologically less active *cis*-isomer (photoinstability), which represents an additional drawback for clinical application [10]. Owing to these pharmacokinetic and physicochemical limitations, current research has increasingly focused on strategies aimed at enhancing the clinical potential of resveratrol. In particular, nanoparticle-based carrier systems offer a rational approach to improve the solubility of resveratrol, slow down its metabolic degradation, protect it against photodegradation, and enhance cellular uptake [10, 12]. Accordingly, the literature reports that resveratrol delivered via nanocarrier systems exhibits higher preclinical biological efficacy compared to its free form [12]. Furthermore, preclinical studies have demonstrated that resveratrol suppresses proliferation in cervical cancer cell lines such as HeLa and is capable of modulating tumor-associated signaling pathways, including transforming growth factor-beta (TGF-β) [13]. Min et al. demonstrated that resveratrol encapsulated in trimethyl chitosan–TPP nanoparticles exhibited enhanced cellular uptake, as well as improved stability and solubility compared to the free form [14]. Similarly, Wu et al. prepared resveratrol-loaded chitosan–TPP nanoparticles and showed that the system not only improved stability under UV exposure and storage conditions but also retained antiproliferative activity in hepatocellular carcinoma cells while reducing toxicity in normal cells [15]. In addition, combination strategies have been developed to enhance the anticancer efficacy of resveratrol by combining it with various natural compounds or chemotherapeutic agents. For example, resveratrol was shown to potentiate the therapeutic efficacy of 5-fluorouracil in colorectal cancer cells [16], its combination with genistein slowed prostate cancer progression [17], and co-administration with curcumin enhanced apoptosis by suppressing proliferation [18]. However, most of these studies were conducted with the free form of these molecules, while combination strategies integrated into polymeric carrier systems, such as chitosan, remain limited. Moreover, surface modifications of chitosan have been reported to play a critical role in drug loading capacity, solubility, and biological interactions [4, 19, 20]. However, most reported chitosan modifications primarily focus on tuning the physicochemical properties of the carrier, whereas the covalent integration of a biologically active small molecule to simultaneously improve carrier performance and contribute to therapeutic efficacy has been less emphasized. In this context, nicotinic acid was employed as a dual-function moiety, serving both as a physicochemical modulator and as a bioactive component capable of enhancing resveratrol's anticancer activity.

In this study, we covalently conjugated nicotinic acid to chitosan to achieve two dual aims: to improve chitosan solubility at physiological pH and to enhance the therapeutic potential of resveratrol through an enhanced combination strategy. In this way, both the carrier properties of chitosan were improved, and a novel anticancer platform was established by combining resveratrol with nicotinic acid. Nicotinic acid (niacin), also known as vitamin B3, is a key precursor in NAD^+ biosynthesis and plays a critical role in maintaining cellular energy metabolism. Recent studies have demonstrated that nicotinic acid is not only a metabolic regulator but also possesses anticancer potential. For example, Li et al. reported that nicotinic acid inhibited glioma cell invasion by degrading Snail1 [21]. Moreover, Subay et al. showed that combining nicotinic acid with rapamycin induced apoptosis and cell cycle arrest in acute myeloid leukemia cell lines [22]. Accordingly, an innovative drug delivery system was developed based on chitosan nanoparticles. Nicotinic acid was covalently conjugated to the chitosan polymer, into which resveratrol was subsequently encapsulated, thereby harnessing the biocompatible carrier properties of chitosan together with the combined anticancer potential of nicotinic acid and resveratrol. Additionally, the ability of nicotinic acid to enhance chitosan solubility at physiological pH was exploited. The synthesized structure was comprehensively characterized by GPC analysis, FTIR, and ^1H NMR spectroscopy, while the encapsulation efficiency, size distribution, and drug release profiles of the nanoparticles were evaluated. Furthermore, the biological effects of the developed system were assessed by evaluating its cytotoxicity against HeLa cervical cancer cells and BJ fibroblasts. This comprehensive approach aims to address the limitations of resveratrol in terms of solubility and bioavailability, to support therapeutic efficacy through the versatile biological activities of nicotinic acid, and to present, for the first time, the combined evaluation of these two natural molecules within the same nanoparticle platform.

2 | Material and Method

2.1 | Chemicals and Reagents

Low molecular weight chitosan (SKU 448869), 1-Ethyl-3-(3-dimethylaminopropyl) carbodiimide hydrochloride (EDC·HCl), and nicotinic acid were obtained from Sigma-Aldrich, USA, for the synthesis of Chi_{Nico}. Glacial acetic acid and sodium tripolyphosphate (TPP) were purchased from Sigma-Aldrich, USA, for chitosan solubilization and crosslinking. Resveratrol (98% purity) was purchased from AmBeed, USA. For cell viability studies, 3-(4,5-dimethylthiazol-2-yl)-2,5-diphenyltetrazolium bromide (MTT) and dimethyl sulfoxide (DMSO) were provided by Sigma-Aldrich, USA, and Minimum Essential Medium Eagle

(MEM-Eagle), penicillin–streptomycin solution, phosphate buffered saline (PBS), fetal bovine serum (FBS), trypsin–EDTA, and L-glutamine were obtained from Biological Industries, Israel.

2.2 | Synthesis and Characterization of Chi_{Nico}

The modification of chitosan with nicotinic acid was performed through a carbodiimide-mediated reaction [23] at a molar ratio of 0.1 mol nicotinic acid/1 mol glucosamine unit. One gram of low molecular weight chitosan was dissolved in 1% (v/v) acetic acid. Separately, a solution of nicotinic acid in water was activated with EDC·HCl (1:1 mmol/mmol) at room temperature for 45 min to activate its carboxyl group. The activated nicotinic acid solution was then added dropwise to the chitosan solution under a nitrogen atmosphere, and the reaction was stirred overnight. The resulting product was dialyzed against deionized water using a 12 kDa MWCO dialysis membrane for 24 h, and the freeze-dried product was stored at +4°C. The synthesis reaction of Chi_{Nico} is shown in Figure 1.

Chi_{Nico} was chemically characterized using the Agilent Cary 630 FTIR spectrometer (USA) and the Varian Unity INOVA ^1H NMR spectrophotometer (Canada) (CD_3COOD-d_6·D_2O, 500 MHz and 25°C). M_w, M_n, and PDI_{Mw} of Chi and Chi_{Nico} were analyzed by GPC–SEC system. This analysis was conducted on a TOSOH EcoSEC system equipped with a refractive index (RI) detector and coupled to a Wyatt miniDAWN Treos II multiangle light scattering (MALS) detector. Separations were carried out using a TSK-gel GMPWXL column operated at 35°C with a flow rate of 0.5 mL/min. An acetic acid/sodium acetate buffer system was employed as the mobile phase. Prior to analysis, all samples were dissolved in acetic acid at a concentration of 4 mg/mL and allowed to equilibrate for 24 h, followed by dilution with sodium acetate solution at a 1:1 (v/v) ratio. The resulting solutions were filtered through a regenerated cellulose (RC) membrane and transferred into vials for injection, after which GPC analysis was carried out.

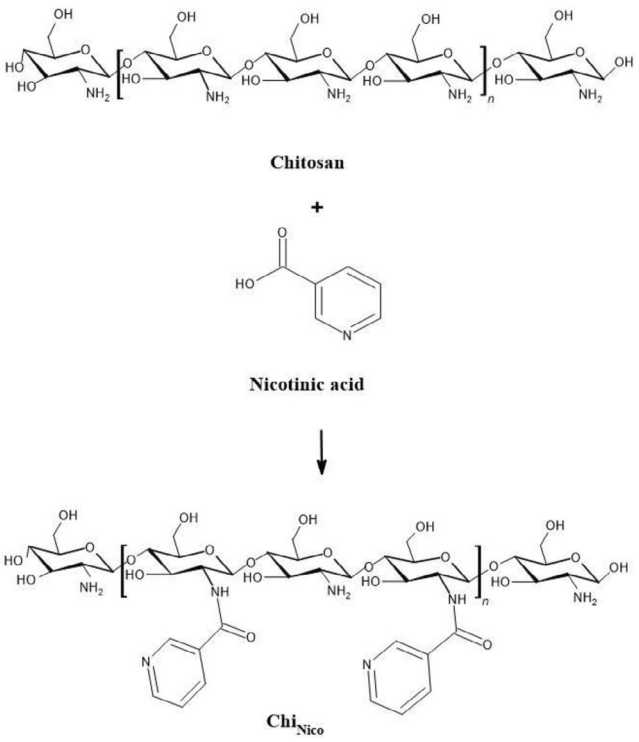

FIGURE 1 | Schematic illustration of nicotinic acid modification of chitosan.

2.3 | Determination of Solubility at Physiological pH

The solubility of Chi and Chi_{Nico} samples at physiological pH (7.4) was evaluated by turbidity [24] methods, which are previously described. In order to evaluate the solubility of Chi and Chi_{Nico} samples by turbidity, the samples were dissolved in 1% (v/v) acetic acid solution at a concentration of 1 mg/mL with stirring for 24 h. The pH of the solutions was then adjusted to 7.4 with 6 N sodium hydroxide, and the turbidity of the resulting dispersion was measured using a UV–vis spectrophotometer at 600 nm. The results were averaged over three independent replicates.

2.4 | Determination of Proton Buffering Capacity

The proton buffering capacities of Chi and Chi_{Nico} were determined by acid–base titration. 6 mg of polymer was dissolved in 150 mM NaCl solution to a concentration of 0.5 mg/mL. After adjusting the pH to 10 with 0.1 M NaOH solution, 20 μL of 0.1 M HCl solution was added and the pH values were recorded. NaCl was used as a negative control group, and the proton buffering capacities of the polymers were calculated from the cumulative HCl volume added until the solution pH dropped from 7.4 to 5, as mmol H^+/1 g polymer [19].

2.5 | Preparation and Characterization of Nanoparticles

Chi and Chi_{Nico} polymers were dissolved separately in a 1% acetic acid solution at a concentration of 3 mg/mL. TPP solution (0.1%, w/v) containing Tween 80 was added dropwise at different ratios (polymer:TPP; 2:1, 3:1, 4:1, and 5:1, w/w) under continuous stirring. The particle size (nm), polydispersity index (PDI), and zeta potential (mV) of the resulting nanoparticles (nChi and $nChi_{Nico}$) were measured using a Horiba SZ-100 instrument after stirring at 250 rpm for 30 min.

In order to prepare RES-loaded nanoparticles ($nChi_{RES}$ and $nChi_{Nico\text{-}RES}$), 100 μL RES dissolved in ethanol (5 mg/mL) was added to the polymer solutions (polymer:RES ratio 10:1), then stirred for 10 min, and the subsequent steps were performed as described above. The resulting nanoparticle formulations contained 1 mg/mL polymer and 0.1% (w/v) Tween 80. Additionally, light scattering of the obtained nanoparticles was visually observed as a result of the Tyndall Effect using a red laser beam (633 nm, 5 mW) [25].

2.6 | Determination of Encapsulation Efficiency of RES-Loaded Nanoparticles

Prepared $nChi_{RES}$ and $nChi_{Nico\text{-}RES}$ formulations were centrifuged at 15,000 rpm for 30 min and the RES encapsulation

efficiencies were determined by measuring the UV absorbance of supernatant with a UV–vis spectrophotometer at 306 nm wavelength. The encapsulation efficiencies of the $nChi_{RES}$ and $nChi_{Nico\text{-}RES}$ were calculated as follows [14]:

$$EE(\%) = \frac{(\text{Total amount RES} - \text{Free amount RES in supernatant})}{\text{Total amount RES}} \times 100 \quad (1)$$

2.7 | In Vitro Release Properties

In vitro RES release studies of $nChi_{RES}$ and $nChi_{Nico\text{-}RES}$ were carried out at pH 7.4 and 5 in PBS containing 0.5% Tween 80 at 37°C. A 12 kDa MWCO dialysis membrane containing 2 mL of $nChi_{RES}$ or $nChi_{Nico\text{-}RES}$ formulation was placed in 47 mL of release medium. Two milliliter aliquots were taken at regular intervals and added each time an equal volume of fresh PBS containing 0.5% Tween 80 into release medium. The amount of RES released from nanoparticles was determined by measuring the UV absorbance of the samples at 306 nm wavelength [15].

2.8 | In Vitro Cytotoxicity Evaluation by MTT Assay

The cytotoxic effects of chitosan-based nanoparticles (nChi and $nChi_{RES}$), nicotinic acid modified chitosan-based nanoparticles ($nChi_{Nico}$ and $nChi_{Nico\text{-}RES}$), and free form RES were evaluated on the HT-29 human colon adenocarcinoma cell line, HeLa cervical adenocarcinoma cell line, and the healthy human fibroblast cell line BJ using the MTT assay. BJ fibroblasts were cultured in MEM-Eagle medium supplemented with 10% FBS, whereas HeLa cells were maintained in MEM-Eagle medium containing 10% FBS and nonessential amino acids. HT-29 colon cancer cells were cultured in RPMI-1640 medium supplemented with 10% FBS. All cell lines were incubated at 37°C in a humidified atmosphere containing 5% CO_2. Cells reaching approximately 90% confluence were detached using trypsin–EDTA, seeded into 96-well plates at a density of 5×10^4 cells per well, and incubated under the same conditions for 24 h to allow adherence. Following adhesion, both cell lines were exposed to chitosan-based nanoparticles containing resveratrol (0.78–50.0 μg/mL) as well as free-form resveratrol for 48 h. To determine cell viability, the medium was removed and MTT solution was added to each well, followed by a 4h incubation. The MTT solution was then removed, and 100 μL of DMSO was added to dissolve the resulting formazan crystals. Absorbance was measured at 570 nm using a microplate reader, and the data were analyzed using GraphPad Prism 8.1 to calculate IC_{50} values and percentage cell viability relative to the negative control [26].

2.9 | Statistical Analysis

All experiments were performed in triplicate unless otherwise stated, and data are presented as mean ± standard deviation (SD). GraphPad Prism 8.0 software was used to perform a two-way analysis of variance (ANOVA) test. ANOVA was applied to assess the effects of treatment and concentration, followed by Dunnett's post hoc multiple comparison test. Statistical significance was defined as a probability value of $p < 0.05$.

3 | Results and Discussion

Chemical modification of chitosan aims to enhance its drug-loading capacity and biological activity. Chitosan, a biocompatible, biodegradable, and low-toxicity biopolymer, possesses primary amine groups that enable covalent bonding with functional molecules [27]. This reactive structure allows controlled regulation of solubility, biological interactions, and release behavior. In particular, selective functionalization of chitosan is crucial for improving pH or redox responsiveness, loading capacity, and targeting ability in drug-delivery systems. Indeed, the literature reports that acylated chitosan exhibits high biocompatibility, enhanced drug-loading capacity, and controlled release properties [4]. In this regard, a Chi_{Nico} conjugate was synthesized through EDC-mediated covalent coupling (amide bond formation) between the free amino groups of chitosan and the carboxyl groups of nicotinic acid. Nicotinic acid, a vitamin B3 derivative, acts as a multifunctional pharmacophore exhibiting diverse biological activities and is noted for its anti-inflammatory and antinociceptive effects [28, 29]. This modification, combined with the natural mucoadhesive and biodegradable properties of chitosan, provides both improved solubility and drug-loading capacity, as well as additional therapeutic potential from the pharmacological activity of nicotinic acid. Moreover, the formation of amide bonds, which are more stable than ester linkages [30], helps maintain structural integrity under physiological conditions and enables a controlled degradation profile for prolonged drug release.

3.1 | Synthesis and Characterization of Chi_{Nico}

3.1.1 | FTIR

The FTIR spectra of chitosan (Chi), nicotinic acid (Nico), and the modified chitosan product (Chi_{Nico}) are presented in Figure 2A,B. In the Chi spectrum (Figure 2A), consistent with previous studies [19, 31], the broad band observed in the range of 3750–3000 cm^{-1} is attributed to the stretching vibrations of primary amine ($-NH_2$) and hydroxyl (–OH) groups. The absorption peaks with max at 2925 and 2883 cm^{-1} correspond to the asymmetric and symmetric stretching vibrations of C–H bonds in the chitosan backbone. Additionally, the short and broad band at 1648 cm^{-1} is assigned to the Amide I (C=O) stretching vibrations, while the shoulder band at 1595 cm^{-1} corresponds to the bending vibrations of primary amine groups. Weak and broad absorptions in the range of 1450–1250 cm^{-1} are associated with the deformation and bending vibrations of methylol (CH_2–OH) groups and the stretching vibrations of $-CH_3$ groups. The broad absorption bands at 1152, 1075, and 1033 cm^{-1} arise from the symmetric and asymmetric stretching vibrations of C–O–C and C–O bonds. In the Nico spectrum (Figure 2A), the long and broad band at 1712 cm^{-1} is attributed to the carbonyl (C=O) stretching vibrations of carboxylic acid groups. The bands in the range of 1595–1417 cm^{-1} correspond to the C=C and C=N stretching vibrations of the pyridine ring, while the short and sharp bands at 1323–1185 cm^{-1} are assigned to C–O stretching vibrations. The absorption bands at 953, 822, and 811 cm^{-1} are related to the deformation vibrations of the aromatic ring [32].

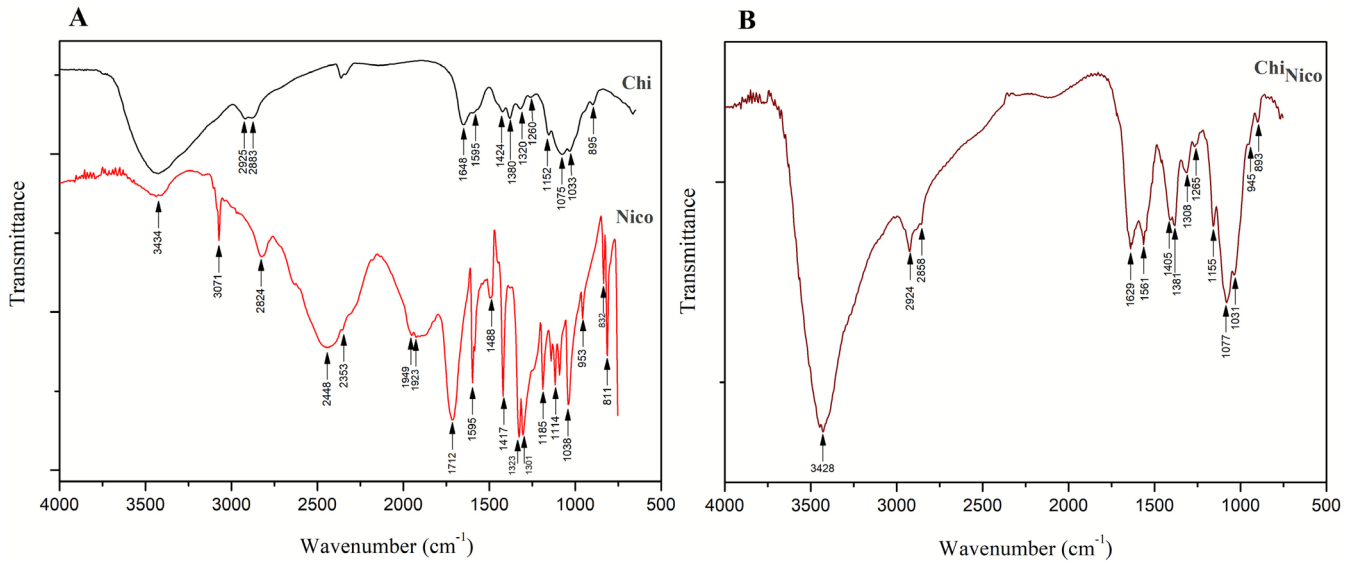

FIGURE 2 | FTIR spectra of (A) Chi and Nico and (B) Chi_{Nico}.

In the Chi_{Nico} spectrum (Figure 2B), the broad band at 3428 cm^{-1} is assigned to the –OH and $–NH_2$ groups present in the structure, and the short shoulder bands at 2924 and 2858 cm^{-1} correspond to C–H stretching vibrations. Compared with Chi, the spectrum of the nicotinic acid-conjugated chitosan product shows the appearance of characteristic absorption peaks in the range of 1650–1620 cm^{-1} corresponding to C=O stretching (Amide I band) and around 1550 cm^{-1} corresponding to C–N–H bending (Amide II band). These changes are manifested by the shift of the Amide I band of Chi from 1648 to 1629 cm^{-1}, the weakening of the amine bending band at 1595 cm^{-1}, and the disappearance of the C=O stretching band of the free carboxylic group of nicotinic acid at 1712 cm^{-1}. Furthermore, the peak observed at approximately 1381 cm^{-1}, which results from the overlap of C–N stretching and N–H bending vibrations (mixed peak, Amide III band), confirms the formation of new amide bonds in the modified product. These spectral changes demonstrate that the amidation (acylation) reaction between the primary amine groups of chitosan and the carboxyl group of nicotinic acid was successfully achieved under EDC (carbodiimide)-mediated activation.

3.1.2 | ^{1}H NMR

^{1}H NMR spectra (500 MHz, D_2O/CD_3COOD) of the Chi_{Nico} is shown in Figure 3. The anomeric protons of chitosan (H-1) appear as a strong multiplet at δ 4.50–5.00 ppm, partially overlapping with the solvent HOD peak. The residual solvent signal appears as the expected HOD peak at $\delta \approx 4.7–4.8$ ppm. The ring-proton envelope characteristic of the glucosamine/GlcNAc backbone is observed at δ 3.95–3.20 ppm (H-3–H-6), with H-2 resonating as a defined signal at δ 3.05–3.15 ppm. The aromatic region (δ 8.6–9.1 ppm) displays three resonances assigned to H-2, H-4, and H-6 of the pyridine ring of nicotinic acid. The presence of these characteristic pyridinyl protons confirms incorporation of the nicotinyl moiety into the polymer structure. Based on integrals of the diagnostic peaks and normalization to H-2 (1 H/repeat), the degree of substitution was calculated as $DS(Nico) = ([1.38 + 2.47 + 1.07]/4)/(23.89/1) = 0.052 \rightarrow 5.2\%$. In the synthesis, nicotinic acid was fed at a molar ratio of 0.1 mol per 1 mol of glucosamine unit, corresponding to a theoretical maximum degree of substitution of 10%. Based on ^{1}H NMR integration, the experimentally determined degree of substitution was 5.2%, indicating an effective grafting efficiency of approximately 52% relative to the feed ratio. This value is fully consistent with the nonquantitative nature of EDC-mediated amidation reactions and further confirms that the coupling reaction proceeds with partial but controlled efficiency.

3.1.3 | GPC

The molecular weight of chitosan is an important factor in nanoparticle-based drug delivery systems, as it affects solubility, viscosity, particle size, drug loading capacity, and release behavior; therefore, its determination by characterization is considered necessary. To evaluate the molecular weight distribution of chitosan after modification, GPC/SEC analysis was performed. The results revealed Mn and Mw values of 100.2 and 319.8 kDa, respectively, corresponding to a polydispersity index (PDI_{Mw}) of 3.191. This relatively high PDI_{Mw} reflects the intrinsic heterogeneity of chitosan, which comprises both shorter and longer polymer chains, and is indicative of a broad molecular-weight distribution [33]. Considering that the native chitosan employed in this study exhibits M_n, M_w, and PDI_{Mw} values of 123.3 kDa, 228.8 kDa, and 1.856, respectively, the observed increase in M_w can be regarded as indirect evidence of the successful conjugation of nicotinic acid to the chitosan backbone. Such a broad molecular weight distribution is characteristic of natural polymer-based systems and is considered typical for chitosan and its derivatives [34, 35].

3.1.4 | Determination of Solubility at Physiological pH

Chitosan dissolves efficiently only under acidic conditions, as its amino groups remain protonated at around pH 6 [36]. At physiological pH, however, deprotonation reduces charge density, resulting in limited solubility and a strong tendency toward aggregation [37]. This inherent limitation has long restricted the broader biomedical application of chitosan, making chemical

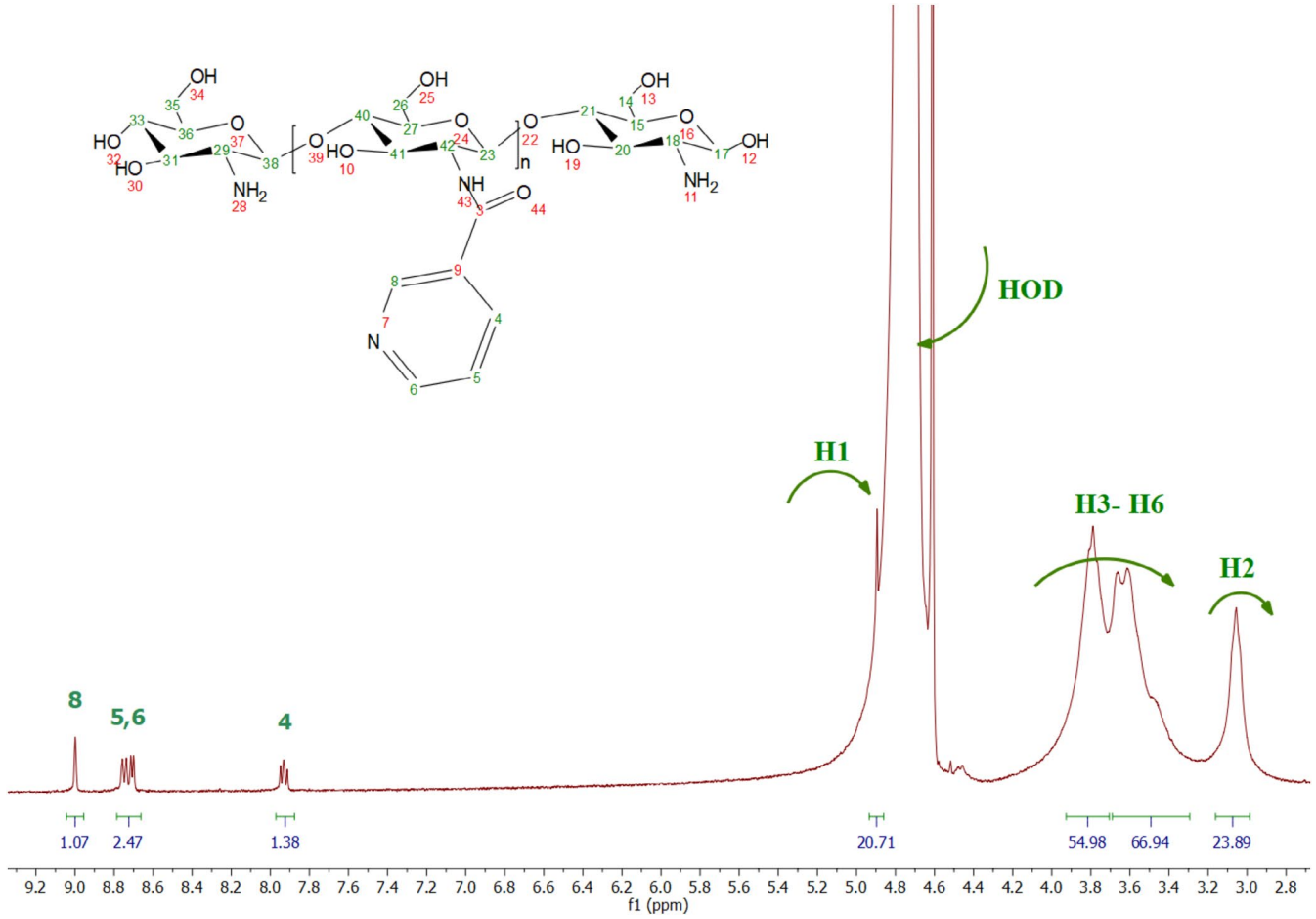

FIGURE 3 | ^{1}H NMR spectra of Chi_{Nico}.

modification a key strategy to improve its performance. In this context, nicotinic acid modification produced a remarkable change in the solubility profile. While native chitosan exhibited excellent solubility at pH 4.0, it rapidly lost this behavior with increasing pH; Chi_{Nico} retained nearly complete solubility even at pH 7.4 (Figure 4A). This observation highlights the profound effect of introducing amidated carboxyl groups and pyridine rings, which can establish additional hydrogen-bonding interactions with water molecules and generate a stable hydration layer around the polymer [38]. At the same time, amidation reduced the number of primary amines, thereby weakening interchain hydrogen bonding and ionic cross-linking that normally stabilize crystalline domains, ultimately rendering the polymer chains more flexible [4]. The steric contribution of the bulky pyridine ring further disrupted tight chain packing, allowing greater molecular free volume and enhanced water penetration. Taken together, these chemical and structural alterations not only alleviate precipitation at neutral pH but also enable chitosan to exhibit a solubility profile at physiological pH that closely resembles its behavior under strongly acidic conditions.

3.1.5 | Determination of Proton Buffering Capacity

One of the critical factors determining the success of a nanoparticle system is its buffering behavior within the lysosomal environment. Following cellular internalization, the decrease in lysosomal pH initiates the degradation of the carrier system [39]. When amino groups present in the polymer backbone become protonated within the pH 5–7.4 range, osmotic pressure increases inside the lysosome, leading to swelling and eventual rupture of the lysosomal membrane [40]. This process prevents the premature degradation of the therapeutic agent under acidic conditions.

Native chitosan, with a buffering capacity of 1.67 mmol H^+/g polymer, provides only limited protection. However, as shown in Figure 4B, nicotinic acid conjugation raised this value to 3 mmol H^+/g polymer. This enhancement can be attributed to the incorporation of pyridine rings, which introduce new protonatable sites, and to amidation, which weakens interchain hydrogen bonding and crystalline domains, thereby increasing the accessibility of residual amino groups. As a result, the number of titratable functional groups effectively contributing to buffering behavior was increased.

This improvement enhances the protection of chitosan nanoparticles against lysosomal degradation. Nevertheless, the obtained capacity remains lower than that of polyethyleneimine (PEI), a polymer well known for its strong buffering behavior, which exhibits a value of 6.3 mmol H^+/g polymer. While the high buffering capacity of PEI provides efficient endosomal escape, it may also induce excessive stability in the cytoplasm, thereby hindering the effective release of the cargo. For this reason, an ideal

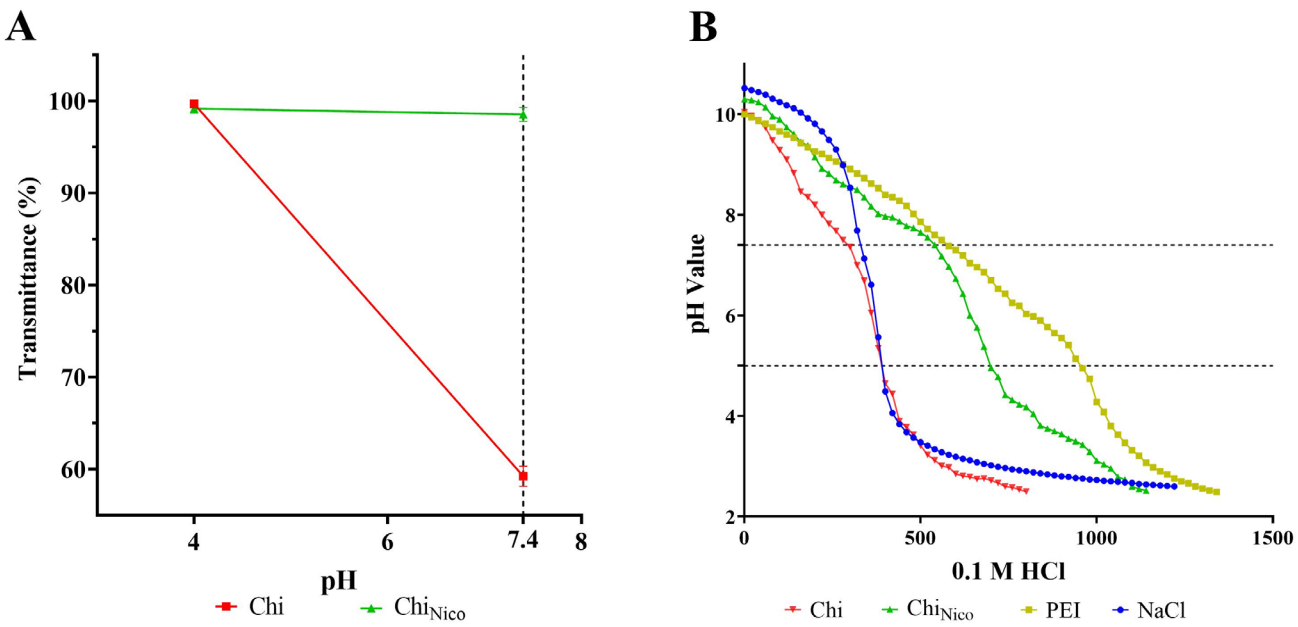

FIGURE 4 | (A) Evaluation of the solubility behavior of Chi and Chi$_{Nico}$ at pH 4.0 and pH 7.4 based on turbidity measurements (B) and titration curves illustrating the buffering behavior of Chi, Chi$_{Nico}$, PEI, and NaCl.

polymeric nanoparticle system should not only protect its cargo from lysosomal degradation but also facilitate its subsequent release into the cytoplasm [41]. Partial degradation of the polymer within the lysosome may even promote cargo release once in the cytoplasm [42]. In this context, the moderate buffering capacity achieved by Chi$_{Nico}$ can be considered a balanced and suitable value for effective intracellular delivery.

3.2 | Preparation and Characterization of the Nanoparticles

In gene or drug delivery applications, intracellular uptake efficiency depends on key physicochemical properties of nanoparticles, including particle size, surface charge (zeta potential), polydispersity index (PDI), solubility, and surface functionality [20]. Evaluating these parameters collectively is critical for predicting the system's behavior in biological environments and its effectiveness as a carrier. Among them, particle size plays a decisive role in determining cellular internalization pathways; literature reports indicate that nanoparticles smaller than 200 nm are more efficiently internalized and exhibit superior distribution within target tissues [31]. Surface charge also directly influences internalization by modulating electrostatic interactions with the cell membrane: a positive zeta potential facilitates cellular entry by generating strong electrostatic attraction with the negatively charged cell membrane, although excessively high positive charges can increase the risk of cytotoxicity due to membrane damage [43]. The PDI reflects the homogeneity of the particle size distribution; lower PDI values (<0.4) indicate a uniform distribution and high colloidal stability, while higher values indicate heterogeneity and a greater tendency toward aggregation [19]. Relatively broad PDI distributions observed in chitosan-based nanoparticle systems are attributed to the intrinsic polymeric nature of chitosan and its varying molecular weight distribution. Increases in chitosan concentration and the degree of functional modification can strengthen intermolecular interactions and hydrogen bonding between polymer chains, which may lead to a limited degree of aggregation during nanoparticle formation [44]. Nevertheless, the PDI values obtained in the present study (around 0.4) are consistent with the range frequently reported in the literature for chitosan-based nanoparticle systems [45, 46].

Chi$_{Nico}$ nanoparticles were prepared via the ionotropic gelation method at different polymer:TPP ratios (w/w). Nanoparticle formation was achieved through the electrostatic interactions between the negatively charged phosphate groups of tripolyphosphate (TPP) and the protonated amino groups of the chitosan backbone, while Tween-80 was employed to stabilize the nanoscale particles. To determine the optimal nanoparticle composition, nChi$_{Nico}$ formulations (n_1Chi$_{Nico}$–n_4Chi$_{Nico}$) were produced at polymer:TPP ratios of 2:1, 3:1, 4:1, and 5:1. As shown in Figure 5A, all formulations with ratios above 2:1 generated large particles of approximately 1 μm in size with PDI values around 1.0. Increasing the Chi$_{Nico}$:TPP ratio led to a tendency toward larger particle sizes and higher PDI values due to the presence of long polymer chains in the dispersion and insufficient crosslinking (Figure 5A,B). Therefore, the 2:1 ratio was selected as optimal, with n_1Chi$_{Nico}$ exhibiting a particle size of 93.43 ± 2.75 nm, a PDI of 0.336 ± 0.019, and a zeta potential of 20.17 ± 0.83 mV, demonstrating physicochemical properties suitable for drug or gene delivery applications.

In addition to common characterization techniques such as dynamic light scattering (DLS), the Faraday–Tyndall effect was employed to confirm the colloidal properties of the nanoparticle systems optically. The Tyndall effect, which occurs when colloidal particles scatter visible light, allows the light path to become visible to the naked eye when particle sizes are smaller than the wavelength of visible light (400–800 nm) and serves as a direct visual indicator of colloidal behavior [47]. In this study, a red laser (633 nm, 5 mW) was used to evaluate the colloidal character of the nanoparticle suspensions. An ethanol solution

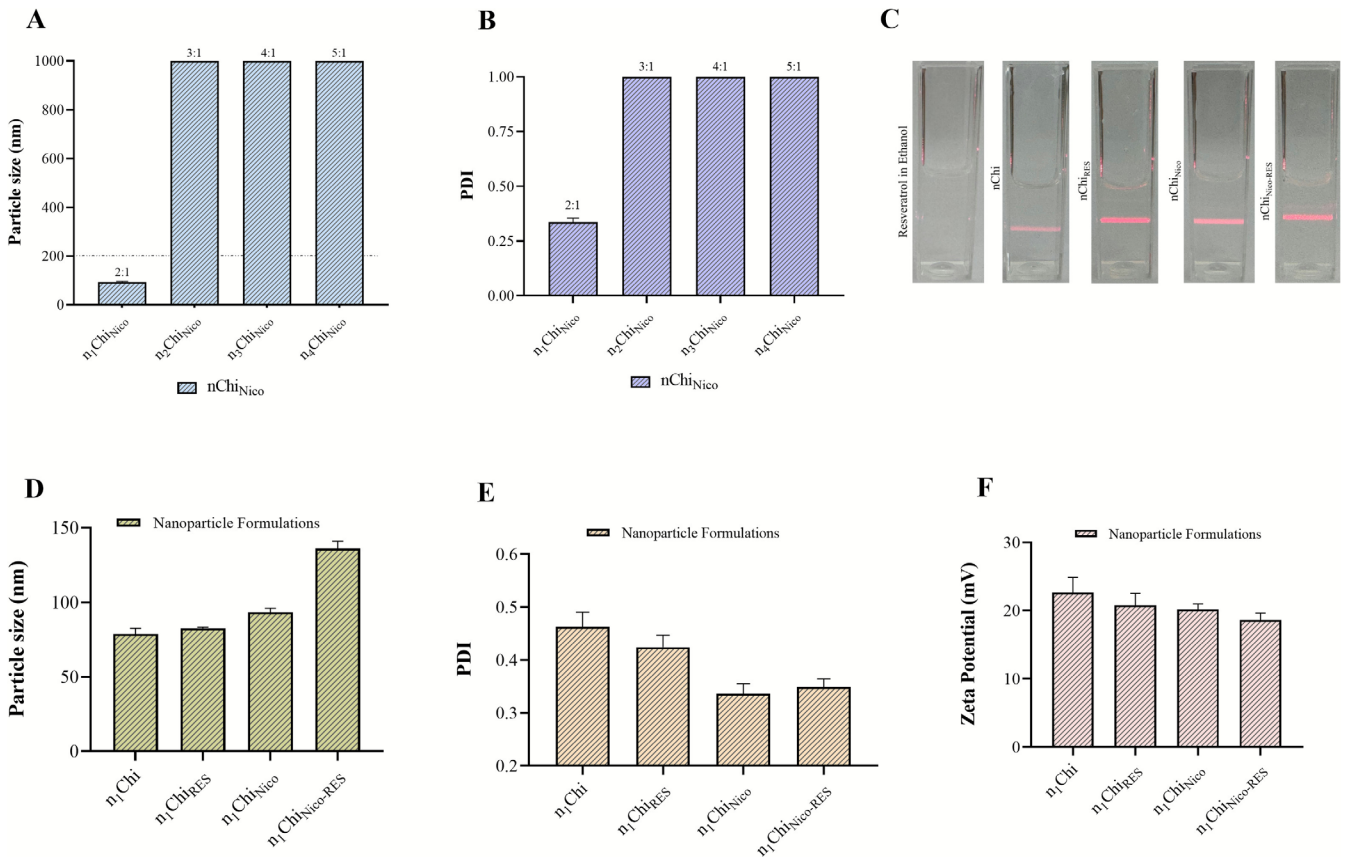

FIGURE 5 | (A) Particle size and (B) PDI of $nChi_{Nico}$. (C) Observation of the Tyndall effect. (D) Particle size, (E) PDI, and (F) zeta potential values of nChi, $nChi_{RES}$, $nChi_{Nico}$, and $nChi_{Nico\text{-}RES}$.

of resveratrol was used as the control group. A distinct light scattering was observed in the nanoparticle suspensions, whereas no scattering was detected in the homogeneous ethanol–resveratrol solution (Figure 5C). These observations confirm the colloidal nature of the nanoparticle systems and visually support the DLS data.

3.3 | RES Loading and Encapsulation Efficiencies of n_1Chi_{RES} and $n_1Chi_{Nico\text{-}RES}$

While preparing RES-loaded nanoparticles, a polymer:TPP ratio of 2:1 was used, which was determined as the optimum ratio for both nChi and $nChi_{Nico}$. RES was added to the nanoparticle formulations at a rate of 10% of the polymer amount. According to DLS measurements, particle size, PDI, and zeta potential values of n_1Chi_{RES} were 82.7 ± 0.7 nm, 0.424 ± 0.023, and 20.8 ± 1.7 mV, respectively. For $n_1Chi_{Nico\text{-}RES}$, these properties were determined as 136.2 ± 4.9 nm, 0.349 ± 0.015, and 18.6 ± 1.0 mV, respectively (Figure 5D–F). The results show that, with RES loading, the particle sizes of both n_1Chi_{RES} and $n_1Chi_{Nico\text{-}RES}$ increased (this ratio was greater in $n_1Chi_{Nico\text{-}RES}$), while the zeta potential values decreased slightly. Nanoparticle size is an important physicochemical property affecting the biocompatibility, absorption, and biological activity of drug carriers [48]. Nanoparticles within the sub-200 nm size range are generally considered suitable for nanomedicine applications based on established design criteria [49]. In this study, both n_1Chi_{RES} and $n_1Chi_{Nico\text{-}RES}$ exhibited particle sizes below 150 nm. As calculated in Equation (1), the encapsulation efficiencies of n_1Chi_{RES} and $n_1Chi_{Nico\text{-}RES}$ were determined as $22.0\% \pm 0.03\%$ and $21.25\% \pm 0.02\%$, respectively.

There are various studies in the literature reporting different encapsulation efficiencies for RES loading into chitosan nanoparticles. It is natural for these studies to yield different encapsulation efficiency values, since, in the case of chitosan nanoparticles, drug encapsulation efficiency is influenced by the degree of deacetylation and average molecular weight of chitosan, solution concentration, the amount of drug, the nanoparticle preparation method, and the parameters associated with these methods [50–52]. In the study conducted by Sposito et al., RES-loaded chitosan nanoparticles achieved an encapsulation efficiency of 72% [53], whereas Bu et al. observed an encapsulation efficiency of approximately 65% [54]. Wu et al. stated in their study investigating the effect of RES concentration on encapsulation efficiency that increasing RES concentration led to a decrease in encapsulation efficiency, and they achieved encapsulation efficiency values of approximately 15.58% [15]. Conte et al. investigated the effects of chitosan solution concentration and crosslinker ratio on encapsulation efficiency and found that the encapsulation efficiency ranged between 16.31% and 76.18% [55]. Jeon et al. stated that, in formulations obtained by ionic gelation with γ-poly(glutamic acid), the RES encapsulation efficiency in chitosan nanoparticles varied between 24% and 35% depending on the amount of γ-poly(glutamic acid) [56]. Je et al. reported in their study investigating the effect of nanoparticle size on encapsulation efficiency that the encapsulation efficiency increased with increasing particle size and varied between 14.88% and 40.86% [57].

3.4 | In Vitro Release Properties of n_1Chi_{RES} and $n_1Chi_{Nico\text{-}RES}$

When the release profiles in Figure 6 are examined, both the n_1Chi_{RES} and $n_1Chi_{Nico\text{-}RES}$ formulations exhibited a rapid release within the first hour, followed by a slower release profile up to 8 h. This type of biphasic release behavior has been widely reported in the literature for chitosan-based nanoparticles [57–61]. During the release experiments, no visible aggregation or precipitation of the nanoparticle dispersions was observed, indicating that the formulations remained physically dispersed in PBS containing 0.5% Tween 80. The initial burst release can be attributed to the desorption of RES weakly adsorbed on the nanoparticle surface, while the subsequent slower phase is governed by diffusion of the drug entrapped within the inner regions of the polymeric matrix [62]. It should be noted that this pronounced initial burst indicates that the present system does not function as a classical long-term sustained-release depot. Instead, it provides rapid initial drug availability, followed by a more gradual release phase, which may be advantageous for achieving an early therapeutic concentration while improving intracellular delivery.

It is also seen that RES release occurs at a higher rate from both the n_1Chi_{RES} and $n_1Chi_{Nico\text{-}RES}$ formulations at pH 7.4 compared to pH 5. The burst release efficiency occurring in the first hour at pH 7.4 is approximately 51% and 58% for n_1Chi_{RES} and $n_1Chi_{Nico\text{-}RES}$, respectively, while these rates are approximately 44% for both formulations at pH 5. This difference in release behavior is due to the interaction between chitosan and TPP molecules. The degree of protonation of the free amine groups of chitosan is lower at pH 7.4 than at pH 5. This causes the electrostatic interaction between the TPP molecules to become weaker and the matrix of the ionically cross-linked nanoparticles to loosen, increasing water penetration. Therefore, RES release occurs at a higher pH 7.4 [63–65]. Additionally, $n_1Chi_{Nico\text{-}RES}$ appears to release slightly higher than n_1Chi_{RES} in both media. This is attributed to the increased hydrophilicity of chitosan following modification with nicotinic acid, facilitating diffusion of the release medium into $n_1Chi_{Nico\text{-}RES}$ matrix and accelerating RES release. Both RES loaded nanoparticle formulations also showed release efficiencies above 90% at both pH 7.4 and 5 after 7 h. This release profile allows RES to reach therapeutic levels quickly.

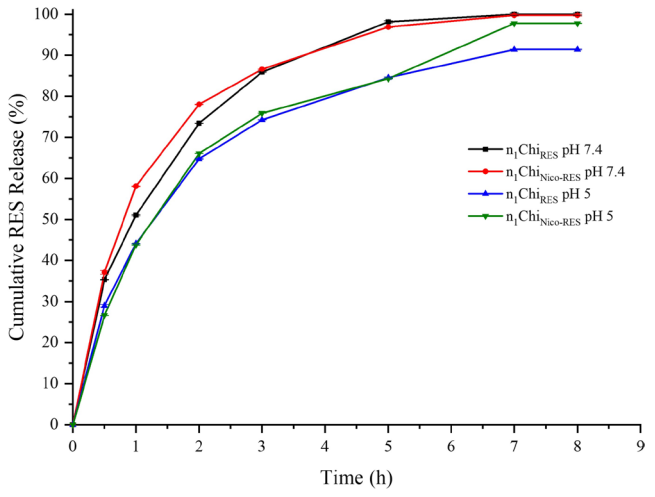

FIGURE 6 | In vitro release profiles of n_1Chi_{RES} and $n_1Chi_{Nico\text{-}RES}$ formulations at pH 7.4 and 5.

3.5 | In Vitro Cytotoxicity Evaluation of Nanoparticles

The cytotoxic effects of chitosan-based nanoparticles (nChi and $nChi_{RES}$), nicotinic acid-modified chitosan-based nanoparticles (n_1Chi_{Nico} and $n_1Chi_{Nico\text{-}RES}$), and free form RES were evaluated on the HeLa cervical adenocarcinoma cell line, HT-29 human colon adenocarcinoma cell line, and the healthy human fibroblast cell line BJ using the MTT assay. Cells were exposed to chitosan-based nanoparticles containing equivalent concentrations of RES (0.78–50.0 μg/mL) and free-form resveratrol for 48 h under incubation conditions. Cell viability was calculated relative to the negative control incubated under the same conditions, without exposure to any substance.

The comparative analysis of cytotoxic effects clearly demonstrates the behaviors of the nanoformulations across HeLa, HT-29, and BJ cells (Figure 7). In HeLa cells (Figure 7B), blank chitosan nanoparticle (nChi) induced only minimal reductions in cell viability, which is consistent with their biocompatible nature. In contrast, both free RES and resveratrol-loaded chitosan nanoparticles ($nChi_{RES}$) displayed dose-dependent cytotoxicity, with $nChi_{RES}$ leading to a slightly stronger effect than free RES, likely due to improved intracellular delivery provided by the nanoparticle system. Similar findings have been reported in previous studies. Bozorgi et al. demonstrated that chitosan/resveratrol polymeric nanoparticles suppressed breast cancer cell proliferation by targeting mitochondrial metabolism and were more effective than free resveratrol [66]. Likewise, Sarma et al. showed that chitosan–pectin core–shell nanoparticles encapsulating resveratrol enhanced stability and antioxidant activity [67]. Wang et al. fabricated zein/carboxymethyl chitosan nanoparticles for co-encapsulation of curcumin and resveratrol, achieving high encapsulation efficiency and preserving bioactivity under storage and digestion conditions [68]. Overall, these studies reinforce the present observations, supporting the conclusion that chitosan encapsulation improves the stability, delivery, and biological performance of resveratrol.

When chitosan was modified with nicotinic acid (n_1Chi_{Nico}) and subsequently loaded with resveratrol ($n_1Chi_{Nico\text{-}RES}$), HeLa cells exhibited a pronounced decrease in viability across all tested concentrations. This suggests that the combination of nicotinic acid and resveratrol within a nanoparticle platform yields enhanced cytotoxicity. Consistent with this, Figure 7A also shows that even blank n_1Chi_{Nico} nanoparticles exert a stronger inhibitory effect on HeLa cell viability than unmodified chitosan nanoparticles, confirming the inherent contribution of nicotinic acid to the overall cytotoxic response. Nicotinic acid itself has been reported to interfere with tumor cell metabolism and signaling pathways. For instance, Li et al. demonstrated that nicotinic acid inhibited glioma cell invasion by degrading Snail1, highlighting its ability to suppress metastatic potential [21]. Similarly, Subay et al. showed that nicotinic acid in combination with rapamycin induced apoptosis and cell cycle arrest in acute myeloid leukemia cells [22]. These findings align with the current results, suggesting that conjugation of nicotinic acid to chitosan may potentiate

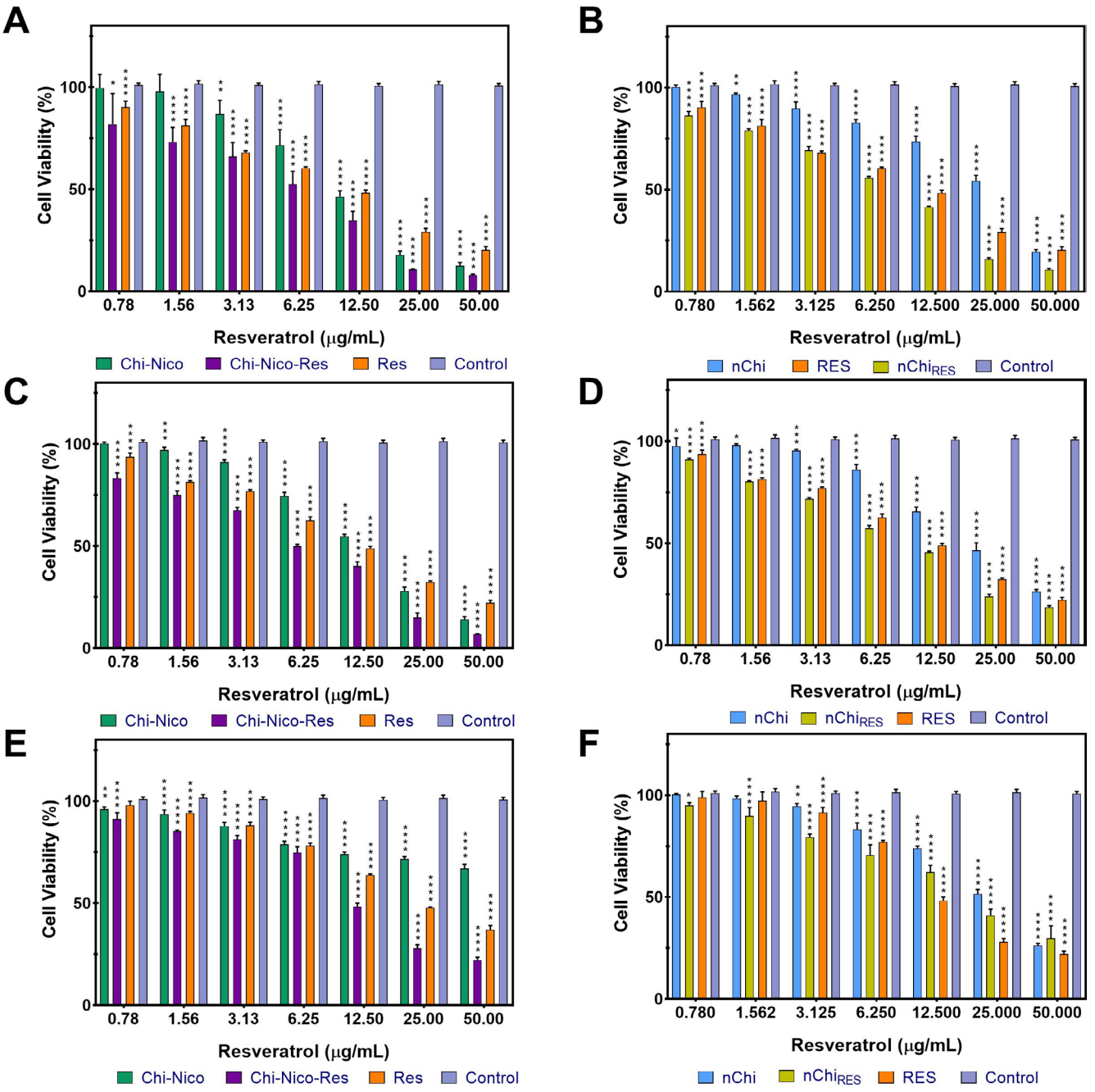

FIGURE 7 | Cytotoxic effects of n_1Chi_{Nico}, $n_1Chi_{Nico\text{-}RES}$, nChi, $nChi_{RES}$, and RES on HeLa cervical adenocarcinoma cell line (A and B), HT-29 colon cancer cell line (C and D), and BJ healthy cell line (E and F). Data represent mean ± SD ($n = 3$ independent experiments). Statistical significance was determined by two-way ANOVA followed by Dunnett's post hoc test (*$p < 0.05$, **$p < 0.01$, ***$p < 0.001$, and ****$p < 0.0001$).

resveratrol's anticancer effects by enhancing cellular uptake and promoting stronger apoptotic signaling.

In HT-29 cells (Figure 7C), a dose-dependent decrease in viability was observed across all treatment groups, attributed to the increasing concentration of RES. However, it is noteworthy that the $n_1Chi_{Nico\text{-}RES}$ group showed significantly higher cytotoxicity compared to free RES and n_1Chi_{Nico}, especially at concentrations of 6.25 μg/mL and above. This suggests that presenting RES within a chitosan-nicotinic acid matrix enhances its antiproliferative activity by increasing intracellular uptake. The limited cytotoxicity of the n_1Chi_{Nico} group alone indicates that the carrier system is largely biocompatible with HT-29 cells.

The effects of chitosan-based nanoparticle formulations, namely nChi, $nChi_{RES}$, and free RES groups, on HT-29 cells were shown in Figure 7D. The significant preservation of cell viability in the nChi group suggests that the nanoparticle carrier is nontoxic. In contrast, a significant and statistically important decrease in cell viability was observed with increasing doses in the $nChi_{RES}$ group. The fact that $nChi_{RES}$ exhibits a stronger cytotoxic effect compared to free RES, particularly at moderate and high concentrations, suggests that nanoparticle-based delivery increases the bioavailability and intracellular activity of RES. The decrease in viability observed in the free RES group was more limited, which may be related to the low solubility and limited intracellular uptake of RES. This study shows that $n_1Chi_{Nico\text{-}RES}$

exhibits a stronger cytotoxic effect in HT-29 cells compared to groups using free RES and the carrier system alone. This increase is particularly pronounced at moderate and high concentrations, suggesting that covalent binding of nicotinic acid to the chitosan chain significantly modulates the biological response.

In literature, nicotinic acid is reported to affect cellular metabolism, NAD^+/NADH balance, and redox homeostasis in cancer cells; these effects can indirectly suppress cell proliferation and apoptotic signaling pathways [69, 70]. Increased energy stress via nicotinamide/NAD^+ metabolism and the limitation of DNA repair mechanisms can make cancer cells more susceptible to cytotoxic agents [71]. In this context, the integration of nicotinic acid into a chitosan carrier can be considered not only a structural modification but also a functional strategy that enhances biological interaction.

In healthy BJ fibroblasts (Figure 7E,F), increasing concentrations of RES, $nChi_{RES}$, and $n_1Chi_{Nico\text{-}RES}$ gradually reduced viability, but the magnitude of cytotoxicity was substantially lower than in HeLa and HT-29 cells. Importantly, although $n_1Chi_{Nico\text{-}RES}$ nanoparticles induced some reduction in BJ fibroblast viability at higher concentrations, the overall effect was less pronounced than in HeLa and HT-29 cells, suggesting that the formulation retains partial biocompatibility and a degree of selectivity toward malignant cells. This contrast between malignant and healthy cells supports the potential of nicotinic acid-modified nanoparticles as more effective and safer anticancer delivery platforms compared to unmodified systems.

The cytotoxic effect of $nChi_{Nico\text{-}RES}$ compared to free resveratrol and unmodified chitosan nanoparticles can be explained by the combination of improved carrier properties and the complementary biological activities of nicotinic acid and resveratrol. Nicotinic acid conjugation significantly improved properties of chitosan such as its solubility at physiological pH and proton buffering capacity; this is expected to facilitate the cellular uptake of the nanoparticles. Furthermore, nicotinic acid plays a role in many pathways in cancer, such as invasion, apoptosis, and cell cycle regulation [21, 22]. In parallel, it is well known that resveratrol induces cancer cell death through ROS-mediated mitochondrial pathways and apoptosis-related signaling [6, 7]. Although direct mechanistic tests were not performed in this study, the stronger reduction in HeLa and HT-29 cell viability observed for $nChi_{Nico\text{-}RES}$, coupled with the moderate cytotoxicity of empty $nChi_{Nico}$ nanoparticles, suggests that nicotinic acid contributes to the overall anticancer response beyond its role as a physicochemical modifier. Taken together, these findings support the idea that the observed improvement results from the combined contribution of enhanced nanoparticle delivery and the intrinsic biological activities of the incorporated bioactive molecule.

4 | Conclusion

In this study, chitosan was covalently conjugated with nicotinic acid, and the combined contribution of this modification to resveratrol delivery was investigated. Nicotinic acid conjugation improved the solubility of chitosan at physiological pH, allowing it to retain a solubility profile comparable to that observed under acidic conditions, while also enhancing its proton buffering capacity and thereby improving its physicochemical and biological performance. The resulting Chi_{Nico} nanoparticles exhibited favorable colloidal properties and an appropriate size distribution for intracellular delivery. Compared with unmodified chitosan formulations, nicotinic acid conjugation slightly increased the particle size of resveratrol-loaded nanoparticles (n_1Chi_{RES}: 82.7 ± 0.7 nm, PDI 0.424 ± 0.023, +20.8 ± 1.7 mV; $n_1Chi_{Nico\text{-}RES}$: 136.2 ± 4.9 nm, PDI 0.349 ± 0.015, +18.6 ± 1.0 mV), while maintaining comparable encapsulation efficiency (22.0% ± 0.03% for n_1Chi_{RES} vs. 21.25% ± 0.02% for $n_1Chi_{Nico\text{-}RES}$). Importantly, resveratrol-loaded Chi_{Nico} nanoparticles produced a relatively stronger reduction in cancer cell lines' viability than both free resveratrol and unmodified chitosan formulations, while cytotoxicity in healthy BJ fibroblasts remained relatively lower. Despite these encouraging results, the current study is limited to physicochemical characterization and in vitro cell-based evaluations. Therefore, further studies involving in vivo models are needed to assess the efficacy, therapeutic significance, and biocompatibility of this system. In conclusion, this study establishes a rational modification strategy for chitosan-based carriers and demonstrates the feasibility of combining nicotinic acid and resveratrol at the cellular level in a single nanoparticle system.

Author Contributions

Sema Şentürk: methodology, visualization, formal analysis, writing – review and editing. **Özlem Kaplan:** methodology, visualization, formal analysis, writing – review and editing. **Kevser Bal:** methodology, visualization, formal analysis, writing – review and editing. **Sibel Küçükertuğrul Çelik:** methodology, visualization, formal analysis, writing – review and editing. **Nazan Gökşen Tosun:** methodology, visualization, formal analysis, writing – review and editing. **Mehmet Koray Gök:** supervision, conceptualization, methodology, investigation.

Funding

This was supported by the project DPT-2019K12-149071 funded by the Presidency of the Republic of Türkiye, Strategy and Budget Office.

Ethics Statement

The authors have nothing to report.

Conflicts of Interest

The authors declare no conflicts of interest.

Data Availability Statement

The data that support the findings of this study are available on request from the corresponding author. The data are not publicly available due to privacy or ethical restrictions.

References

1. B. Wang, S. Hu, Y. Teng, et al., "Current Advance of Nanotechnology in Diagnosis and Treatment for Malignant Tumors," *Signal Transduction and Targeted Therapy* 9, no. 1 (2024): 200.

2. L. Ding, P. Agrawal, S. K. Singh, Y. S. Chhonker, J. Sun, and D. J. Murry, "Polymer-Based Drug Delivery Systems for Cancer Therapeutics," *Polymers* 16, no. 6 (2024): 843.

3. K. Elumalai, S. Srinivasan, and A. Shanmugam, "Review of the Efficacy of Nanoparticle-Based Drug Delivery Systems for Cancer Treatment," *Biomedical Technology* 5 (2024): 109–122.

4. K. Bal, S. Küçükertuğrul Çelik, S. Şentürk, Ö. Kaplan, E. B. Eker, and M. K. Gök, "Recent Progress in Chitosan-Based Nanoparticles for Drug Delivery: A Review on Modifications and Therapeutic Potential," *Journal of Drug Targeting* 33, no. 8 (2025): 1366–1393.

5. E. Ribeiro and N. Vale, "The Role of Resveratrol in Cancer Management: From Monotherapy to Combination Regimens," *Targets* 2, no. 4 (2024): 307–326.

6. L. Kursvietiene, D. M. Kopustinskiene, I. Staneviciene, et al., "Anti-Cancer Properties of Resveratrol: A Focus on Its Impact on Mitochondrial Functions," *Antioxidants* 12, no. 12 (2023): 2056.

7. E. M. Varoni, A. F. Lo Faro, J. Sharifi-Rad, and M. Iriti, "Anticancer Molecular Mechanisms of Resveratrol," *Frontiers in Nutrition* 3 (2016): 1–15.

8. M. Annaji, I. Poudel, S. H. S. Boddu, R. D. Arnold, A. K. Tiwari, and R. J. Babu, "Resveratrol-Loaded Nanomedicines for Cancer Applications," *Cancer Reports* 4, no. 3 (2021): e1353.

9. A.-M. Trofin, D. V. Scripcariu, S.-I. Filipiuc, et al., "From Nature to Nanomedicine: Enhancing the Antitumor Efficacy of Rhein, Curcumin, and Resveratrol," *Medicina* 61, no. 6 (2025): 981.

10. N. Summerlin, E. Soo, S. Thakur, Z. Qu, S. Jambhrunkar, and A. Popat, "Resveratrol Nanoformulations: Challenges and Opportunities," *International Journal of Pharmaceutics* 479, no. 2 (2015): 282–290.

11. C. K. Singh, M. A. Ndiaye, and N. Ahmad, "Resveratrol and Cancer: Challenges for Clinical Translation," *Biochimica et Biophysica Acta* 1852, no. 6 (2015): 1178–1185.

12. A. Arabzadeh, T. Mortezazadeh, T. Aryafar, E. Gharepapagh, M. Majdaeen, and B. Farhood, "Therapeutic Potentials of Resveratrol in Combination With Radiotherapy and Chemotherapy During Glioblastoma Treatment: A Mechanistic Review," *Cancer Cell International* 21, no. 1 (2021): 391.

13. R. Hussein Khalaf and Z. Hosseini Khah, "The Effect of Resveratrol on Cervical Cancer Cell Growth by Inhibiting TGF-β Gene Expression," *Journal of Obstetrics, Gynecology and Cancer Research* 11, no. 1 (2026): 10–16.

14. J. B. Min, E. S. Kim, J. S. Lee, and H. G. Lee, "Preparation, Characterization, and Cellular Uptake of Resveratrol-Loaded Trimethyl Chitosan Nanoparticles," *Food Science and Biotechnology* 27, no. 2 (2018): 441–450.

15. J. Wu, Y. Wang, H. Yang, X. Liu, and Z. Lu, "Preparation and Biological Activity Studies of Resveratrol Loaded Ionically Cross-Linked Chitosan-TPP Nanoparticles," *Carbohydrate Polymers* 175 (2017): 170–177.

16. S. S. Chung, P. Dutta, D. Austin, P. Wang, A. Awad, and J. V. Vadgama, "Combination of Resveratrol and 5-Flurouracil Enhanced Anti-Telomerase Activity and Apoptosis by Inhibiting STAT3 and Akt Signaling Pathways in Human Colorectal Cancer Cells," *Oncotarget* 9, no. 68 (2018): 32943–32957.

17. C. E. Harper, L. M. Cook, B. B. Patel, et al., "Genistein and Resveratrol, Alone and in Combination, Suppress Prostate Cancer in SV-40 Tag Rats," *Prostate* 69, no. 15 (2009): 1668–1682.

18. C. Li, Y. Xu, J. Zhang, et al., "The Effect of Resveratrol, Curcumin and Quercetin Combination on Immuno-Suppression of Tumor Microenvironment for Breast Tumor-Bearing Mice," *Scientific Reports* 13, no. 1 (2023): 13278.

19. K. Bal, Ö. Kaplan, S. Şentürk, S. Küçükertuğrul Çelik, K. Demir, and M. K. Gök, "Improving Physiological Solubility and Gene Transfer Efficiency of Chitosan via 3-Nitrobenzaldehyde and Amino Acid Conjugation," *International Journal of Biological Macromolecules* 323 (2025): 147117.

20. Y. Tantan, Ö. Kaplan, K. Bal, et al., "Tricine-Modified Chitosan as a Strategy for Enhancing Hydrophilicity and Gene Delivery," *Carbohydrate Research* 547 (2025): 109326.

21. J. Li, J. Qu, Y. Shi, et al., "Nicotinic Acid Inhibits Glioma Invasion by Facilitating Snail1 Degradation," *Scientific Reports* 7, no. 1 (2017): 43173.

22. L. B. Subay, E. B. Gencer Akçok, and İ. Akçok, "Rapamycin and Niacin Combination Induces Apoptosis and Cell Cycle Arrest Through Autophagy Activation on Acute Myeloid Leukemia Cells," *Molecular Biology Reports* 52, no. 1 (2024): 75.

23. E. B. E. Fidan, K. Bal, and S. K. Pabuccuoğlu, "A Review on Basic Principles of Mucoadhesion: The Importance of Chitosan as a Mucoadhesive Biopolymer," *ALKÜ Fen Bilimleri Dergisi* 6, no. 3 (2024): 174–194.

24. C. Qin, H. Li, Q. Xiao, Y. Liu, J. Zhu, and Y. Du, "Water-Solubility of Chitosan and Its Antimicrobial Activity," *Carbohydrate Polymers* 63, no. 3 (2006): 367–374.

25. K. Yuan, Y. Sun, F. Liang, et al., "Tyndall-Effect-Based Colorimetric Assay With Colloidal Silver Nanoparticles for Quantitative Point-of-Care Detection of Creatinine Using a Laser Pointer Pen and a Smartphone," *RSC Advances* 12, no. 36 (2022): 23379–23386.

26. K. Bal, M. K. Gök, K. Demir, and S. Özgümüş, "Building Effective Nanocarriers Based on β-Ionone Loaded 2nd and 3rd Generation L-Arginine Dendrimers: In Vitro Evaluation of Cytotoxicity and Antiproliferative Activity for HeLa Cells," *Materials Today Chemistry* 44 (2025): 102545.

27. K. Szczubialka, K. Zomerska, A. Karewicz, and M. Nowakowska, "Novel Drug Carrier—Chitosan Gel Microspheres With Covalently Attached Nicotinic Acid," *Journal of Controlled Release* 116, no. 2 (2006): e13–e15.

28. R. Shamsheer, S. Sunoqrot, V. Kasabri, et al., "Preparation and Characterization of Capsaicin Encapsulated Polymeric Micelles and Studies of Synergism With Nicotinic Acids as Potential Anticancer Nanomedicines," *Journal of Pharmacy & Bioallied Sciences* 15, no. 3 (2023): 107–125.

29. S. Manturthi, D. Bhattacharya, K. R. Sakhare, K. P. Narayan, and S. V. Patri, "Nicotinic Acid-Based Cationic Vectors for Efficient Gene Delivery to Glioblastoma Cells," *New Journal of Chemistry* 46, no. 43 (2022): 20886–20899.

30. M. Winnacker and B. Rieger, "Poly (Ester Amide): Recent Insights Into Synthesis, Stability and Biomedical Applications," *Polymer Chemistry* 7, no. 46 (2016): 7039–7046.

31. S. Çelik, M. K. Gök, K. Demir, S. Pabuccuoğlu, and S. Özgümüş, "Relationship Between Phosphorylamine-Modification and Molecular Weight on Transfection Efficiency of Chitosan," *Carbohydrate Polymers* 277 (2022): 118870.

32. H. Yang, Y. Lu, L. Bao, Y. Liu, D. Liu, and Z. Zhong, "Preparation and Bioactivities of Chitosan Nicotinamide Derivatives and Their Application in the Preservation of Cherry Tomatoes," *International Journal of Food Microbiology* 434 (2025): 111149.

33. I. Aranaz, A. R. Alcántara, M. C. Civera, et al., "Chitosan: An Overview of Its Properties and Applications," *Polymers* 13, no. 19 (2021): 3256.

34. R. Román-Doval, S. P. Torres-Arellanes, A. Y. Tenorio-Barajas, A. Gómez-Sánchez, and A. A. Valencia-Lazcano, "Chitosan: Properties and Its Application in Agriculture in Context of Molecular Weight," *Polymers* 15, no. 13 (2023): 2867.

35. K. Piekarska, M. Sikora, M. Owczarek, J. Jóźwik-Pruska, and M. Wiśniewska-Wrona, "Chitin and Chitosan as Polymers of the Future—Obtaining, Modification, Life Cycle Assessment and Main Directions of Application," *Polymers* 15, no. 4 (2023): 793.

36. I. A. Sogias, V. V. Khutoryanskiy, and A. C. Williams, "Exploring the Factors Affecting the Solubility of Chitosan in Water," *Macromolecular Chemistry and Physics* 211, no. 4 (2010): 426–433.

37. S. Suryani, A. Y. Chaerunisaa, I. M. Joni, et al., "The Chemical Modification to Improve Solubility of Chitosan and Its Derivatives Application, Preparation Method, Toxicity as a Nanoparticles," *Nanotechnology, Science and Applications* 17 (2024): 41–57.

38. Q. Li, C. Zhang, W. Tan, G. Gu, and Z. Guo, "Novel Amino-Pyridine Functionalized Chitosan Quaternary Ammonium Derivatives: Design, Synthesis, and Antioxidant Activity," *Molecules* 22, no. 1 (2017): 156.

39. N. Desai, D. Rana, S. Salave, D. Benival, D. Khunt, and B. G. Prajapati, "Achieving Endo/Lysosomal Escape Using Smart Nanosystems for Efficient Cellular Delivery," *Molecules* 29, no. 13 (2024): 3131.

40. M. K. Gök, "In Vitro Evaluation of Synergistic Effect of Primary and Tertiary Amino Groups in Chitosan Used as a Non-Viral Gene Carrier System," *European Polymer Journal* 115 (2019): 375–383.

41. M. Thibault, S. Nimesh, M. Lavertu, and M. D. Buschmann, "Intracellular Trafficking and Decondensation Kinetics of Chitosan-pDNA Polyplexes," *Molecular Therapy* 18, no. 10 (2010): 1787–1795.

42. M. Thibault, M. Lavertu, M. Astolfi, and M. D. Buschmann, "Structure Dependence of Lysosomal Transit of Chitosan-Based Polyplexes for Gene Delivery," *Molecular Biotechnology* 58, no. 10 (2016): 648–656.

43. I. Demir, S. Küçükertuğrul Çelik, K. Bal, et al., "Enhancing Transfection Efficiency of Primary Cell Lines Using Different Terminated PBAE Structures Without Endcapping Reaction," *Colloid and Polymer Science* 303 (2025): 1–15.

44. D. Ghosh and K. Kuotsu, "Development, Characterization and In Vitro Evaluation of Capecitabine Loaded Chitosan Nanoparticles," *Drug Development and Industrial Pharmacy* 51, no. 8 (2025): 1–13.

45. P. Patel, N. O. Shoyele, and S. A. Shoyele, "Preparation and Evaluation of Meclinertant-Loaded PLGA/Chitosan Nanoparticles as a Potential Treatment for Non-Small Cell Lung Cancer Using A549 Cells," *Journal of Drug Delivery Science and Technology* 107 (2025): 106831.

46. A. M. Dos Santos, R. B. Liszbinski, S. G. Carvalho, et al., "5-Fluorouracil-Loaded Chitosan Nanoparticles Conjugated With Methotrexate for Targeted Therapy of Colorectal Cancer," *International Journal of Biological Macromolecules* 287 (2025): 138342.

47. L. F. Aguilera, L. O. Araujo, W. M. Facchinatto, et al., "Blue-Light Photoactivated Curcumin-Loaded Chitosan Nanoparticles Prepared by Nanoprecipitation and Ionic Gelation: A Promising Approach for Antimicrobial Photodynamic Inactivation," *ACS Applied BioMaterials* 8, no. 5 (2025): 4055–4064.

48. Z. Zhang, M. Ge, D. Wu, et al., "Resveratrol-Loaded Sulfated Hericium Erinaceus β-Glucan-Chitosan Nanoparticles: Preparation, Characterization and Synergistic Anti-Inflammatory Effects," *Carbohydrate Polymers* 332 (2024): 121916.

49. Z. Zhao, A. Ukidve, V. Krishnan, and S. Mitragotri, "Effect of Physicochemical and Surface Properties on In Vivo Fate of Drug Nanocarriers," *Advanced Drug Delivery Reviews* 143 (2019): 3–21.

50. Y. Herdiana, E. Febrina, S. Nurhasanah, D. Gozali, K. M. Elamin, and N. Wathoni, "Drug Loading in Chitosan-Based Nanoparticles," *Pharmaceutics* 16, no. 8 (2024): 1043.

51. S. H. Bidooki, L. Spitzer, A. Petitpas, et al., "Chitosan Nanoparticles, a Novel Drug Delivery System to Transfer Squalene for Hepatocyte Stress Protection," *ACS Omega* 9, no. 52 (2024): 51379–51393.

52. S. Sanyakamdhorn, D. Agudelo, and H.-A. Tajmir-Riahi, "Encapsulation of Antitumor Drug Doxorubicin and Its Analogue by Chitosan Nanoparticles," *Biomacromolecules* 14, no. 2 (2013): 557–563.

53. L. Spósito, D. Fonseca, S. G. Carvalho, et al., "Engineering Resveratrol-Loaded Chitosan Nanoparticles for Potential Use Against *Helicobacter pylori* Infection," *European Journal of Pharmaceutics and Biopharmaceutics* 199 (2024): 114280.

54. L. Bu, L.-C. Gan, X.-Q. Guo, et al., "Trans-Resveratrol Loaded Chitosan Nanoparticles Modified With Biotin and Avidin to Target Hepatic Carcinoma," *International Journal of Pharmaceutics* 452, no. 1–2 (2013): 355–362.

55. R. Conte, I. De Luca, A. Valentino, et al., "Hyaluronic Acid Hydrogel Containing Resveratrol-Loaded Chitosan Nanoparticles as an Adjuvant in Atopic Dermatitis Treatment," *Journal of Functional Biomaterials* 14, no. 2 (2023): 82.

56. Y. O. Jeon, J.-S. Lee, and H. G. Lee, "Improving Solubility, Stability, and Cellular Uptake of Resveratrol by Nanoencapsulation With Chitosan and γ-Poly (Glutamic Acid)," *Colloids and Surfaces B: Biointerfaces* 147 (2016): 224–233.

57. H. J. Je, E. S. Kim, J.-S. Lee, and H. G. Lee, "Release Properties and Cellular Uptake in Caco-2 Cells of Size-Controlled Chitosan Nanoparticles," *Journal of Agricultural and Food Chemistry* 65, no. 50 (2017): 10899–10906.

58. N. D. Machado, M. A. Fernández, and D. D. Díaz, "Recent Strategies in Resveratrol Delivery Systems," *ChemPlusChem* 84, no. 7 (2019): 951–973.

59. A. R. Cho, Y. G. Chun, B. K. Kim, and D. J. Park, "Preparation of Chitosan–TPP Microspheres as Resveratrol Carriers," *Journal of Food Science* 79, no. 4 (2014): E568–E576.

60. P. Hasanzade, G. Mosayebi, A. Ganji, S. Fahimirad, and A. Ghazavi, "Curcumin-Loaded Chitosan Nanoparticles: A Promising Approach to Liver Fibrosis Prevention," *BMC Pharmacology and Toxicology* 26, no. 1 (2025): 190.

61. K. S. Yadav, H. P. Nijhawan, P. Nirale, D. Singhal, and G. Soni, "Efficient Nose-To-Brain Delivery of Chitosan-Coated Resveratrol Nanoemulsion in Rats: Formulation Optimized Using D-Optimal Mixture Design," *Journal of Dispersion Science and Technology*, ahead of print, March 24, 2025.

62. Y. Zu, Y. Zhang, W. Wang, et al., "Preparation and In Vitro/In Vivo Evaluation of Resveratrol-Loaded Carboxymethyl Chitosan Nanoparticles," *Drug Delivery* 23, no. 3 (2016): 971–981.

63. A. Alishahi, A. Mirvaghefi, M. Tehrani, et al., "Shelf Life and Delivery Enhancement of Vitamin C Using Chitosan Nanoparticles," *Food Chemistry* 126, no. 3 (2011): 935–940.

64. K. V. Jardim, J. L. N. Siqueira, S. N. Báo, and A. L. Parize, "In Vitro Cytotoxic and Antioxidant Evaluation of Quercetin Loaded in Ionic Cross-Linked Chitosan Nanoparticles," *Journal of Drug Delivery Science and Technology* 74 (2022): 103561.

65. R. Ghosh, S. Mondal, D. Mukherjee, et al., "Oral Drug Delivery Using a Polymeric Nanocarrier: Chitosan Nanoparticles in the Delivery of Rifampicin," *Materials Advances* 3, no. 11 (2022): 4622–4628.

66. A. Bozorgi, Z. Haghighi, M. R. Khazaei, M. Bozorgi, and M. Khazaei, "The Anti-Cancer Effect of Chitosan/Resveratrol Polymeric Nanocomplex Against Triple-Negative Breast Cancer: An In Vitro Assessment," *IET Nanobiotechnology* 17, no. 2 (2023): 91–102.

67. S. Sarma, S. Agarwal, P. Bhuyan, J. Hazarika, and M. Ganguly, "Resveratrol-Loaded Chitosan–Pectin Core–Shell Nanoparticles as Novel Drug Delivery Vehicle for Sustained Release and Improved Antioxidant Activities," *Royal Society Open Science* 9, no. 2 (2022): 210784.

68. P. Wang, Y. Yin, Y. Zhang, and J. Shao, "Fabrication and Characterization of Zein/Carboxymethyl Chitosan Nanoparticles for Co-Encapsulation of Curcumin and Resveratrol," *Frontiers in Nutrition* 12 (2025): 1–11.

69. A. Chiarugi, C. Dölle, R. Felici, and M. Ziegler, "The NAD Metabolome—A Key Determinant of Cancer Cell Biology," *Nature Reviews Cancer* 12, no. 11 (2012): 741–752.

70. L. E. Navas and A. Carnero, "Nicotinamide Adenine Dinucleotide (NAD) Metabolism as a Relevant Target in Cancer," *Cells* 11, no. 17 (2022): 2627.

71. E. Fouquerel and R. W. Sobol, "ARTD1 (PARP1) Activation and NAD+ in DNA Repair and Cell Death," *DNA Repair* 23 (2014): 27–32.